Intercomparison of SCIAMACHY and OMI tropospheric NO$_2$ columns: Observing the diurnal evolution of chemistry and emissions from space

K. Folkert Boersma,[1,2] Daniel J. Jacob,[1] Henk J. Eskes,[3] Robert W. Pinder,[4,5] Jun Wang,[1] and Ronald J. van der A[3]

[1] Concurrent (August 2006) measurements of tropospheric NO$_2$ columns from OMI aboard Aura (1330 local overpass time) and SCIAMACHY aboard Envisat (1000 local overpass time) offer an opportunity to examine the consistency between the two instruments under tropospheric background conditions and the effect of different observing times. For scenes with tropospheric NO$_2$ columns <5.0 × 10^{15} molecules cm^{-2}, SCIAMACHY and OMI agree within 1.0–2.0 × 10^{15} molecules cm^{-2}, consistent with the detection limits of both instruments. We find evidence for a low bias of 0.2 × 10^{15} molecules cm^{-2} in OMI observations over remote oceans. Over the fossil fuel source regions at northern midlatitudes, we find that SCIAMACHY observes up to 40% higher NO$_2$ at 1000 local time (LT) than OMI at 1330 LT. Over biomass burning regions in the tropics, SCIAMACHY observes up to 40% lower NO$_2$ columns than OMI. These differences are present in the spectral fitting of the data (slant column) and are augmented in the fossil fuel regions and dampened in the tropical biomass burning regions by the expected increase in air mass factor as the mixing depth rises from 1000 to 1330 LT. Using a global 3-D chemical transport model (GEOS-Chem), we show that the 1000–1330 LT decrease in tropospheric NO$_2$ column over fossil fuel source regions can be explained by photochemical loss, dampened by the diurnal cycle of anthropogenic emissions that has a broad daytime maximum. The observed 1000–1330 LT NO$_2$ column increase over tropical biomass burning regions points to a sharp midday peak in emissions and is consistent with a diurnal cycle of emissions derived from geostationary satellite fire counts.

1. Introduction

[2] Nitrogen oxides (NO$_x$ = NO + NO$_2$) play an important role in atmospheric chemistry. Near the Earth's surface, emissions of NO$_x$ in the presence of hydrocarbons and sunlight lead to the urban and regional-scale formation of ozone. In the presence of ammonia (NH$_3$), oxidation of NO$_x$ to nitric acid leads to the formation of aerosol nitrate (NH$_4$NO$_3$). Both ozone as well as fine particles at ground levels have a detrimental effect on public health. Moreover, there is a general interest in NO$_x$ as the limiting precursor for ozone in the global troposphere, as ozone is an efficient greenhouse gas and a source of hydroxyl (OH). To obtain a better understanding of how NO$_x$ is influencing air pollution and contributing to the greenhouse effect, accurate and precise measurements of NO$_x$ over large spatial domains with sufficient temporal sampling are indispensable.

[3] Ground-based and airborne measurements of NO$_x$ are temporally and spatially limited. Satellite instruments provide measurements with global coverage and fixed spatial and temporal resolution. Data sets of tropospheric NO$_2$ columns retrieved from the Global Ozone Monitoring Experiment (GOME), the Scanning Imaging Absorption Chartography (SCIAMACHY) and the Ozone Monitoring Experiment (OMI) now span more than 10 years (1996–2006) and have been used for trend studies [*Richter et al.*, 2005; *van der A et al.*, 2006a]. GOME and SCIAMACHY tropospheric NO$_2$ data has been used to estimate surface emissions of NO$_x$ [*Martin et al.*, 2003; *Jaeglé et al.*, 2004, 2005; *Müller and Stavrakou*, 2005; *Bertram et al.*, 2005; *Toenges-Schüller et al.*, 2006; *Konovalov et al.*, 2006; *Martin et al.*, 2006; *Kim et al.*, 2006] and lightning NO$_x$

---

[1]School of Engineering and Applied Sciences, Harvard University, Cambridge, Massachusetts, USA.

[2]Now at Royal Netherlands Meteorological Institute, De Bilt, Netherlands.

[3]Royal Netherlands Meteorological Institute, De Bilt, Netherlands.

[4]Atmospheric Sciences Modeling Division, Air Resources Laboratory, NOAA, Research Triangle Park, North Carolina, USA.

[5]National Exposure Research Laboratory, U.S. Environmental Protection Agency, Research Triangle Park, North Carolina, USA.

production [*Boersma et al.*, 2005; *Beirle et al.*, 2006; *Martin et al.*, 2007].

[4] The latest generation of satellite instruments observes the Earth with horizontal resolutions that allow a detailed view of the NO$_x$ pollution patterns. SCIAMACHY [*Bovensmann et al.*, 1999] on board ESA's Envisat has a horizontal resolution of 30 × 60 km^2 and OMI [*Levelt et al.*, 2006] on board NASA's EOS-Aura satellite has a nadir pixel size of 13 × 24 km^2. There is a growing interest from various environmental and public health agencies to start using these satellite observations to verify emission inventories, investigate trends in emissions, and forecast air quality. It is important to obtain confidence in the satellite observations by validation and error characterization. The quality of SCIAMACHY NO$_2$ data retrieved by KNMI/BIRA has previously been validated by *Petritoli et al.* [2005], *Schaub et al.* [2007] and *Blond et al.* [2007], with SCIAMACHY columns generally being within 20% of the validation data. Furthermore, near-real-time OMI NO$_2$ retrievals from KNMI [*Boersma et al.*, 2007] are shown to be consistent within 5% with aircraft vertical profiles during the INTEX-B campaign in situations where assumptions on the unobserved part of the troposphere are limited [*Boersma et al.*, 2008].

[5] We present here an intercomparison of SCIAMACHY and OMI observations using similar KNMI retrievals. The consistency of the SCIAMACHY and OMI retrievals greatly facilitates our intercomparison, as it minimizes differences in retrieval assumptions that potentially lead to large systematic differences between retrievals [*van Noije et al.*, 2006]. Of particular interest is to interpret the comparison in terms of the implied diurnal variation of NO$_x$ emissions and chemistry. Both SCIAMACHY and OMI are in sun-synchronous orbits, with equator crossing times of 1000 and 1330 local time (LT) at subsatellite point respectively. NO$_x$ emissions from transport are expected to peak during the morning commute, while power plants and industrial sources have in general little diurnal variation. Fire and soil emissions are expected to peak in the middle of the day. Chemical loss of NO$_x$ also peaks in the middle of the day. Resolving the compounded effects of these different diurnal variations is critical for the application of satellite observations to estimate NO$_x$ emissions, although this has not been properly recognized in previous studies. The different overpass times of SCIAMACHY and OMI offer an opportunity to test our current understanding.

2. SCIAMACHY and OMI Tropospheric NO$_2$ Retrievals

2.1. Common Algorithm

[6] SCIAMACHY and OMI are UV/Vis spectrometers that measure direct sunlight and backscattered light from the Earth's atmosphere. We use a common algorithm for the retrieval of SCIAMACHY and OMI tropospheric NO$_2$ columns. Slant columns of NO$_2$ are obtained by fitting the absorption cross-section spectra of NO$_2$ to the observed reflectance spectra (defined as the ratio between the Earth radiance and solar irradiance spectra) around 440 nm. The retrieved slant column represents the column of NO$_2$ (in molecules per cm^2) along the average photon path from the Sun, through the atmosphere, to the satellite instrument.

[7] To convert retrieved slant columns into vertical, tropospheric NO$_2$ columns (N_v), we follow the approach described by *Boersma et al.* [2004]:

$$N_v = \frac{N_s - N_{s,st}}{M_{tr}}, \qquad (1)$$

where $N_{s,st}$ is the stratospheric component of the NO$_2$ slant column N_s, and M_{tr} represents the tropospheric air mass factor (AMF) that depends on viewing geometry, cloud fraction, cloud pressure, surface albedo, and the a priori NO$_2$ profile.

[8] For both SCIAMACHY and OMI retrievals, we estimate the stratospheric slant column by data assimilation of NO$_2$ slant columns in the TM4 chemical transport model (CTM) [*Dentener et al.*, 2003]. The estimate of stratospheric NO$_2$ thus adjusts to observed NO$_2$ over regions dominated by stratospheric NO$_2$ (e.g., oceans), while stratospheric winds in TM4 ensure the propagation of the assimilated information. See *Boersma et al.* [2007] for more details.

[9] Removal of the stratospheric slant column $N_{s,st}$ from the total slant column N_s defines the tropospheric slant column, which we convert to the tropospheric vertical column by applying the tropospheric AMF (M_{tr}) as in equation (1). We compute tropospheric AMFs following the formulation of *Palmer et al.* [2001] and *Eskes and Boersma* [2003] with the DAK radiative transfer model [*Stammes*, 2001], accounting for solar and viewing zenith angle (at the surface), and relative azimuth angle, and furthermore take into account the effects of clouds (for SCIAMACHY from the FRESCO [*Koelemeijer et al.*, 2001] and for OMI from the O$_2$-O$_2$ [*Acarreta et al.*, 2004] cloud algorithm), surface albedo (from the *Herman and Celarier* [1997] and *Koelemeijer et al.* [2002] data sets as described *Boersma et al.* [2004]), and the a priori vertical profile shape from TM4. No independent aerosol correction is applied as it is effectively accounted for in the cloud retrievals as shown in [*Boersma et al.*, 2004].

[10] A crucial aspect in comparing SCIAMACHY and OMI NO$_2$ sets, is that they be retrieved in a consistent manner. Slant columns have been retrieved by nonlinear least-square fitting of backscattered radiance spectra for both SCIAMACHY (by BIRA, the Belgian Institute for Space Aeronomy) and OMI (by KNMI/NASA). For both retrievals, we use the data assimilation of slant columns in TM4 to estimate the stratospheric columns. The AMFs have been computed with the same radiative transfer model, the same surface albedo data set, and the same TM4 model to obtain vertical profile shapes. Cloud information is taken from the FRESCO and O$_2$-O$_2$ algorithms that are based on the same set assumptions (i.e., clouds are modeled as Lambertian reflectors with albedo 0.8). Both SCIAMACHY and OMI retrievals account for the temperature dependence of the NO$_2$ absorption cross-section spectrum using actual ECMWF temperature information following *Boersma et al.* [2004]. Here we have used version 1.04 of the KNMI/BIRA SCIAMACHY and version 0.9 of the KNMI/NASA OMI retrievals. Some aspects pertaining to the retrievals are characteristic to each instrument, and we give here a short overview of the main differences.

Table 1. Instrument Characteristics Relevant for SCIAMACHY and OMI NO$_2$ Retrievals

Instrument	Satellite	Local Equator Crossing Time	Nadir Field of View	Global Coverage	Spectral Range	Spectral Resolution (at 440 nm)
SCIAMACHY	Envisat	1000	30×60 km^2	6 d	220–2380 nm	0.44 nm
OMI	EOS-Aura	1330	13×24 km^2	1 d	270–500 nm	0.63 nm

2.2. Differences Between SCIAMACHY and OMI

2.2.1. Instrumental Differences

[11] Table 1 gives an overview of essential instrumental characteristics of the SCIAMACHY and OMI tropospheric NO$_2$ retrievals. Important differences are:

[12] 1. The horizontal resolution of SCIAMACHY nadir viewing scenes (pixels) when the instrument is in nominal operation mode is 30×60 km^2. The horizontal resolution of OMI in nominal operations mode is 13×24 km^2 for scenes observed with a viewing angle of 0° (nadir) to approximately 135×26 km^2 for scenes observed at the edges of the swath with a satellite viewing angle of 57° (M. Dobber, personal communication, 2007).

[13] 2. SCIAMACHY alternately takes limb and nadir measurements. The observations in the limb mode are not sensitive to the troposphere so that tropospheric (nadir) NO$_2$ retrievals from SCIAMACHY are not continuous. This, combined with SCIAMACHY's field of view that corresponds to 960 km on the Earth's surface, leads to a global coverage that is achieved within approximately 6 d. OMI has a 114° field of view, which corresponds to an approximately 2600 km wide swath on the Earth's surface. Because of the wide swath of the 14–15 orbits per day, OMI achieves global coverage in 1 d.

[14] 3. SCIAMACHY measures direct and backscattered solar radiation between 220 nm and 2380 nm with a spectral resolution of 0.44 nm around 440 nm. OMI measures between 270 and 500 nm, so that cloud retrieval using the O$_2$ A-band (760 nm) is not possible with OMI, and the O$_2$-O$_2$ absorption feature (470 nm) is used instead.

2.2.2. Retrieval Differences

[15] Table 2 summarizes the main differences in the fitting procedures followed for SCIAMACHY and OMI. NO$_2$ retrievals from SCIAMACHY are the result of a collaboration between KNMI and BIRA. Slant columns are obtained by BIRA by fitting a modeled spectrum to the measured reflectance in the 426.3–451.3 nm region. For OMI, a wider fit window (405–465 nm) is used to account for lower signal-to-noise ratios (~1400 for nominal midlatitude conditions) than in SCIAMACHY measurements (signal-to-noise ~2000). In the work by *Boersma et al.* [2002], we did not find a strong sensitivity of the OMI fitting results for various combinations of fitting windows,

fitting techniques, or inclusion of species with minor absorption features such as H$_2$O and O$_2$-O$_2$. Different NO$_2$ absorption spectra are used in SCIAMACHY [*Bogumil et al.*, 2003] and OMI [*Vandaele et al.*, 1998] but the differences are less than 2% at all temperatures, affecting differences in the temperature correction [*Boersma et al.*, 2004] in the SCIAMACHY and OMI retrievals by at most 2%. We do not expect significant differences between SCIAMACHY and OMI slant columns from the fitting differences in Table 2 or from the temperature correction. We investigate the combined effect of differences in the fitting methods and the postfitting temperature correction in section 3, where we compare SCIAMACHY and OMI total, stratospheric and tropospheric slant NO$_2$ columns.

[16] In the first stages of its operational lifespan, SCIAMACHY reflectances have been found to be systematically underestimated by approximately 13% [*Acarreta and Stammes*, 2005], largely because of radiometric offsets in solar irradiances [*Skupin et al.*, 2005]. Because of this lack of usable solar spectra, KNMI/BIRA retrievals use a radiance spectrum over the Indian Ocean as the reference spectrum. This reference spectrum is assumed to contain the signature of a 1.5×10^{15} molecules cm^{-2} vertical stratospheric NO$_2$ column [*van der A et al.*, 2006b]. For reasons of consistency, this reference spectrum has continued to be used for SCIAMACHY retrievals, even after high-quality irradiance measurements became available. Moreover, the use of a radiance measurement as reference spectrum for SCIAMACHY ensures long-term consistency with KNMI/BIRA retrievals for GOME. For OMI, a solar irradiance spectrum is used for the spectral fitting procedure, and a correction for a NO$_2$ signature in the reference spectrum is not necessary.

[17] Calibration errors in the OMI reflectance measurements lead to spurious across-track variability. This variability is significantly reduced, but not removed altogether, by the correction procedure described by *Boersma et al.* [2007]. Any residual error that remains after the correction procedure is an implicit part of the OMI slant column error estimate of 0.7×10^{15} molecules cm^{-2} [*Boersma et al.*, 2007] that we use in the remainder of the manuscript.

[18] Cloud parameters for SCIAMACHY and OMI are retrieved with algorithms that are somewhat different. A

Table 2. Spectral Fitting Characteristics for SCIAMACHY and OMI NO$_2$ Retrievals

Instrument	SCIAMACHY	OMI
Fitting window	426.3–451.3 nm	405.0–465.0 nm
Signal-to-noise[a]	~2000	~1400
Fitted species	NO$_2$, O$_3$, Ring, O$_2$-O$_2$, H$_2$O	NO$_2$, O$_3$, Ring
Spectral resolution	0.44 nm	0.63 nm
Fitting method	nonlinear least squares	nonlinear least squares
NO$_2$ cross section spectrum	SCIAMACHY PFM [*Bogumil et al.*, 2003]	*Vandaele et al.* [1998] convolved with OMI ITF[b]

[a]Approximate ratio's for nominal midlatitude conditions.
[b]*Dirksen et al.* [2006].

comparison of the FRESCO and O$_2$-O$_2$ cloud algorithms [*Boersma et al.*, 2007] showed that mean cloud fractional cover, on average, agreed to within 1.1% (absolute values). Cloud pressures from the O$_2$-O$_2$ algorithm (OMI) were found to be higher (+58 hPa) than from FRESCO (SCIAMACHY). The implications of the differences in cloud parameters will be discussed in section 4.

[19] Local overpass times can vary within a subsatellite track and cover two (SCIAMACHY) or sometimes three (OMI) time zones. In principle, our 1000–1330 LT comparison could be affected by the effect of different overpass time. In practice, this effect is small and in any case not systematic. Some OMI observations will have times of 1200 LT, others 1500 LT, but the ensemble of OMI observations is representative for 1330 LT. Furthermore, there is a higher probability for detecting cloud-free situations in small nadir (1330 LT overpass) pixels than in the larger-sized pixels at the edges of the swath (1200 or 1500 LT), and this effectively reduces the potential effect of different overpass times. The effect of different OMI overpass times within a track could be reduced altogether by excluding off-nadir observations at the expense of loss of collocated observations.

3. Intercomparison of SCIAMACHY and OMI Tropospheric NO$_2$ Columns

[20] Figure 1 shows the monthly mean tropospheric NO$_2$ fields derived from SCIAMACHY and OMI for August 2006, averaged over 0.5° × 0.5° grid cells. Cloud screening was performed for both SCIAMACHY and OMI. In order to assure that the dominant part of the observed signal originates indeed from the cloud-free part of the pixel, only observations with cloud radiance fractions less than 50% were included in the average. This ensures that only those (cloud-free) OMI observations have been used that are spatially coincident with (cloud-free) SCIAMACHY observations taken on the same day. Cloud information has been obtained with the FRESCO and O$_2$-O$_2$ algorithms for SCIAMACHY and OMI, respectively, and both cloud fraction and cloud pressure are fully accounted for in the retrieval as discussed in section 2.1.

[21] The spatial distributions of SCIAMACHY and OMI monthly mean tropospheric NO$_2$ columns have a correlation coefficient $r = 0.77$ ($n = 1.9 \times 10^{15}$). Both observe the highest values over the urban regions of North America, Europe, and China, and also high levels over the biomass burning regions of South America, southern Africa, and Indonesia. The OMI mean tropospheric NO$_2$ field is much smoother than that of SCIAMACHY because it is based on more pixels.

[22] Figure 2 shows absolute differences between the SCIAMACHY and OMI monthly mean tropospheric NO$_2$ columns for August 2006, and Figure 3 shows the corresponding scatterplot. We estimate a 1-sigma uncertainty for individual retrievals as the sum of a base absolute component (from spectral fitting and the stratospheric background) and a relative component from the AMF [*Boersma et al.*, 2004, 2007]. For OMI, the base component is 0.5–1.5 × 10^{15} molecules cm^{-2} (depending on the AMF). For SCIAMACHY retrievals, which have a better fitting precision, the base component is 0.3–1.0 × 10^{15} molecules

cm^{-2}. Following *Boersma et al.* [2007], we adopt a relative (AMF) component of ∼30%, so that the total error for individual retrievals is approximated by 0.65 × 10^{15} + 0.3 × N_v (SCIAMACHY) and 1.0 × 10^{15} molecules cm^{-2} + 0.3 × N_v (OMI).

[23] SCIAMACHY NO$_2$ is generally higher than OMI over fossil fuel source regions, which is particularly pronounced in large urban areas such as megacities (Los Angeles, Mexico City, Moscow, Riyadh, Tehran, Hong Kong). This would be expected from the combination of morning peak in emissions and midday maximum in NO$_x$ chemical loss. In contrast, OMI observes higher NO$_2$ columns over biomass burning regions in Brazil, southern Africa, and Indonesia, and we attribute this to a midday peak in emissions as discussed below. In some cases values from OMI are higher than SCIAMACHY downwind of isolated urban areas (this is particularly manifest for Riyadh and the Highveld Plateau area), which could reflect transport of the urban plume. Another area where OMI is higher than SCIAMACHY is the southeastern United States, and possible reasons for this will be discussed below.

[24] Figure 3 summarizes the differences between global monthly mean SCIAMACHY and OMI NO$_2$ columns in August 2006. The scatter between SCIAMACHY and OMI data results from the combined uncertainty (random errors given above) in both retrievals. The dashed-dotted lines in Figure 3 show the error bounds computed from the combined (theoretical) uncertainty for monthly mean SCIAMACHY and OMI averages at 0.5° × 0.5°. The error bounds are based on estimated uncertainties for (1) SCIAMACHY of $\frac{0.65 \times 10^{15} + 0.3 \times N_v}{\sqrt{3}}$, with the denominator taking into account the averaging over multiple days (in this case on average 3) in August 2006 and for (2) OMI of $\frac{1.0 \times 10^{15} + 0.3 \times N_v}{\sqrt{3}\sqrt{3.5}}$, with the denominator taking into account the averaging over multiple days and multiple pixels (on average, an OMI pixel is 3.5 times smaller than a SCIAMACHY pixel). For tropospheric columns <3.0 × 10^{15} molecules cm^{-2} (where the running average shows no appreciable bias; 76% of all grid cells), 68% of the observed scatter is within the error bounds, consistent with expectations for a normal distribution of errors with some error correlation (through the AMF) between the two instruments. For tropospheric columns >3.0 × 10^{15} molecules cm^{-2}, SCIAMACHY tropospheric NO$_2$ columns are, on average, higher than OMI and for columns >8.0 × 10^{15} molecules cm^{-2} even well beyond the combined uncertainties of the two retrievals.

[25] Figure 4a shows the probability distribution functions (PDFs) for the monthly mean SCIAMACHY and OMI data sets. The median of the OMI PDF is left-shifted by 0.2 × 10^{15} molecules cm^{-2} relative to SCIAMACHY. This bias is a background feature, as shown in Figure 4b by a PDF subset for the clean Pacific Ocean. We find that OMI NO$_2$ within this region is on average 0.17 × 10^{15} molecules cm^{-2} lower than SCIAMACHY, and the mean is negative. We conclude that OMI suffers from a small negative bias over unpolluted regions. We find a similar negative bias from a validation study over the remote Gulf of Mexico [*Boersma et al.*, 2008]. The negative bias is also apparent in Figures 1 and 2 as a stronger land-sea contrast in tropospheric NO$_2$ columns for OMI than for SCIAMACHY, especially over
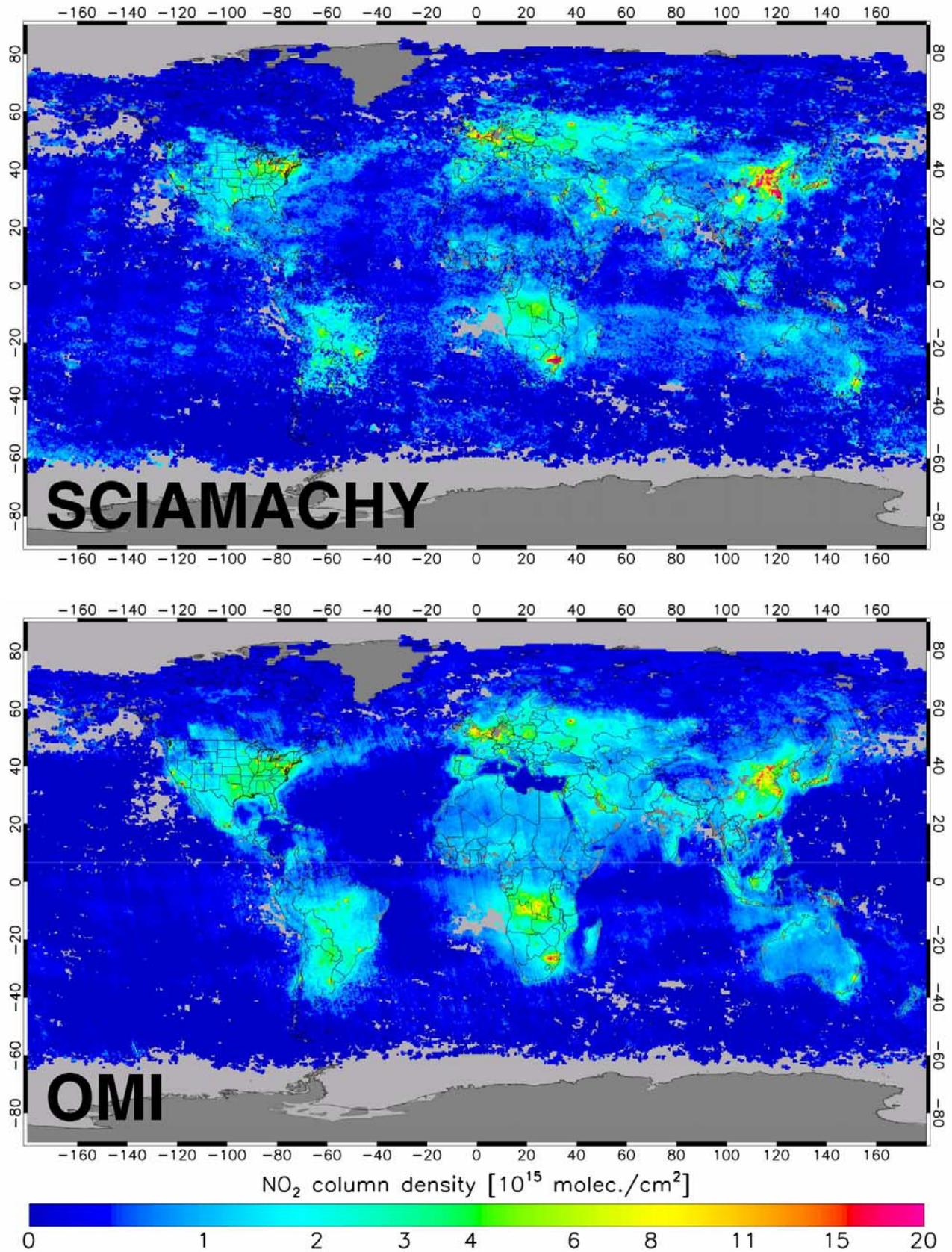
Figure 1. Monthly mean tropospheric NO$_2$ columns in August 2006 from SCIAMACHY and OMI, in situations when both observe a mostly clear (cloud radiance fraction <50%) scene. Grey grid cells were not observed or had persistent cloud cover.
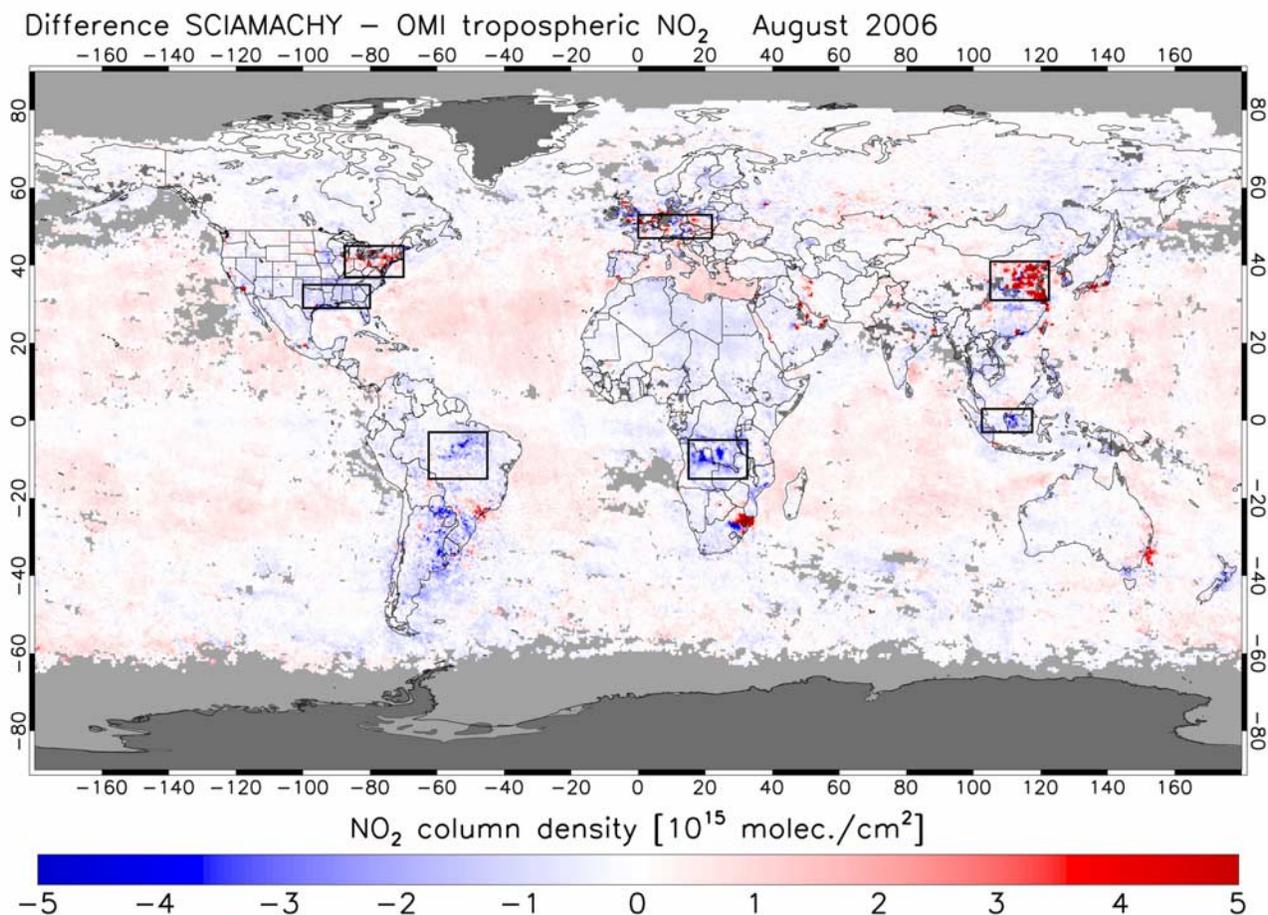
Figure 2. Absolute difference between monthly mean SCIAMACHY and OMI tropospheric NO₂ columns for August 2006. Red colors indicate higher retrievals from SCIAMACHY than from OMI, and vice versa for blue colors. The black rectangles enclose the regions studied in section 5.

the Mediterranean region. This bias is inconsequential for polluted regions.

[26] Negative tropospheric NO₂ columns may occur if the slant stratospheric column exceeds the total slant column (see equation (1)). This would be caused by a bias in the assimilation procedure used for the stratospheric column estimate. Figure 5 shows that SCIAMACHY (normalized) total slant columns are systematically smaller than OMI (normalized) total slant columns; that is, the distribution of differences peaks at -0.59×10^{15} molecules cm^{-2}. This is likely due to the differences in reference spectrum for the SCIAMACHY (backscatter spectrum with residual NO₂ signature) and OMI (solar irradiance spectrum) spectral fitting procedures (see section 2.2.2). Figure 5 also shows that the differences between SCIAMACHY and OMI total slant columns are closely followed by the differences between SCIAMACHY and OMI (geometric AMF-normalized) stratospheric slant columns. On average, (SCIAMACHY-OMI) stratospheric slant column differences are -0.58×10^{15} molecules cm^{-2}, very close to the slant column differences. This is expected from the assimilation procedure: biased slant columns propagate into similarly biased stratospheric slant columns (described in

section 2.1). The relative bias between SCIAMACHY and OMI cancels (equation (1)) and only marginally affects the tropospheric slant columns for any of the two data sets. This is confirmed by the curve with the solid line in Figure 5 that shows a median difference corresponding to zero.

4. SCIAMACHY Versus OMI Differences in NO$_x$ Source Regions

[27] We now investigate the cause of the large differences between OMI and SCIAMACHY over polluted and biomass burning regions (Figure 2). A first issue is to determine whether they are driven by differences in tropospheric slant columns ($N_s - N_{s,st}$, hereafter slant columns) or in AMFs. Difference in the slant columns points to information in the actual spectra, while difference in the AMF points to information in the physics of the retrieval (such as higher mixing depths at 1330 LT than at 1000 LT). As slant columns and AMFs are both proportional to the length of the light path, we normalize them by the local geometrical AMF, ($M_g = \frac{1}{\cos(\theta)} + \frac{1}{\cos(\theta_0)}$ where θ is the satellite viewing angle and θ_0 is the solar zenith angle) to remove the simple
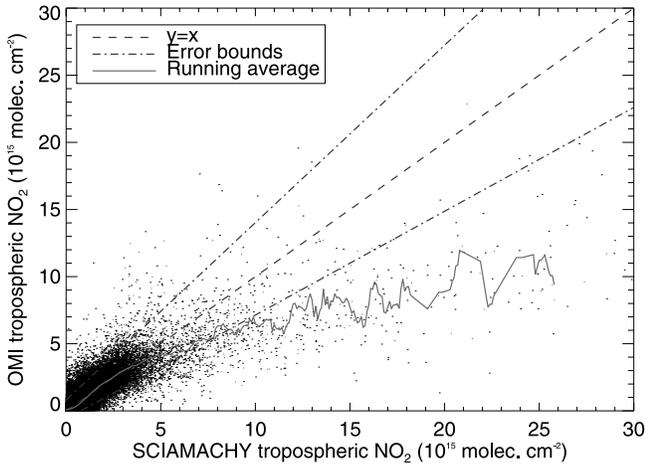
Figure 3. Scatterplot of OMI versus SCIAMACHY tropospheric NO$_2$ columns in August 2006. Each point represents the monthly mean for a $0.5° \times 0.5°$ grid cell. The dashed-dotted lines show the error bounds from the combined uncertainties in the SCIAMACHY and OMI retrievals. The red line shows the OMI running average over 0.5×10^{15} molecules cm^{-2} wide SCIAMACHY NO$_2$ bins.

effect of optical geometry. Tropospheric vertical columns (N_v) can thus be expressed as:

$$N_v = \frac{N_s - N_{s,st}}{M_g} \frac{M_g}{M_{tr}} \qquad (2)$$

Here, $\frac{N_s - N_{s,st}}{M_g}$ and $\frac{M_{tr}}{M_g}$ are the normalized slant columns, and normalized AMFs, respectively. We successively examine these two terms, focusing on the NO$_x$ source regions delineated by boxes in Figure 2.

[28] Table 3 shows the ratio of observed SCIAMACHY and OMI tropospheric NO$_2$ columns for regions with strong NO$_x$ sources where we observe the largest differences between SCIAMACHY and OMI tropospheric NO$_2$ columns, and the contributions from the slant column and the AMF, for the source regions of Figure 2. For the fossil fuel source regions where SCIAMACHY is higher than OMI, slant columns and AMFs both make comparable compounding contributions to the difference in tropospheric columns. For the biomass burning and southeastern United States regions where OMI is higher than SCIAMACHY, the difference is mainly in the slant columns with only a small effect from the AMFs.

[29] The AMF difference between SCIAMACHY and OMI deserves some discussion. Both AMF calculations use the same surface albedos [*Herman and Celarier*, 1997; *Koelemeijer et al.*, 2002] and the cloud fractions are similar within 1%. Moreover, the differences between SCIAMACHY and OMI cloud fractions do not correlate with the differences between SCIAMACHY and OMI tropospheric NO$_2$ columns (not shown). Thus the normalized AMF differences in Table 3 must reflect either differences in cloud-top pressures or in the NO$_2$ vertical shape profile. The OMI and SCIAMACHY cloud retrieval algorithms show a small difference in cloud-top pressure, with OMI on average higher by 60 hPa [*Boersma et al.*, 2007].

Since temporal variation in global cloud fraction and cloud-top pressure between 1000 and 1330 LT is small [*Bergman and Salby*, 1996], this difference represents an algorithmic bias. *Boersma et al.* [2004, Figure 5b] shows increasing AMFs with increasing cloud-top pressure, especially for situations with low clouds and polluted boundary layers. Since we exclude scenes with cloud radiance fractions >50%, the impact of systematically different cloud-top pressures on AMF calculations remains limited. To investigate the effect of the cloud-top pressure bias, we computed AMFs with different cloud-top pressures (OMI +60 hPa) but otherwise identical forward model parameters (albedo, cloud fraction, and profile shape) as in the actual retrievals for August 2006, and find OMI AMFs to be higher by up to 10% for scenes with high NO$_2$.

[30] Both SCIAMACHY and OMI use the TM4 CTM to estimate vertical NO$_2$ profiles, and growth of the atmospheric mixed layer between 1000 and 1330 LT would lead to a greater vertical extent of NO$_2$ seen by OMI and hence a higher AMF. In TM4, boundary layer mixing follows the vertical diffusion parameterization of *Holtslag and Moeng* [1991]. Diffusion coefficients and mixing depths are updated every 3 h as described by *Krol et al.* [2005]. To investigate the effect of increased mixing layer depth, we compared tropospheric AMFs computed with NO$_2$ profiles sampled at 1000 and at 1330 LT, but otherwise identical forward model parameters (albedo and cloud inputs) as in the actual retrievals for August 2006. We find tropospheric AMFs to be up to 15% larger at 1330 LT than at 1000 LT.

[31] In conclusion, it is clear that the differences between SCIAMACHY and OMI in source regions cannot be ascribed to a retrieval artifact. Most of the difference is in the spectra. Although the retrieval (through the AMF) contributes to the lower tropospheric columns in OMI for a given slant column, this mostly reflects well understood physics of diurnal mixed layer growth. We now turn to explaining these differences on the basis of diurnal variation in NO$_x$ emissions and chemistry.

5. Diurnal Variations in Tropospheric NO$_2$ Columns

5.1. Model Versus Satellite Observations

[32] We use the global GEOS-Chem CTM (see Appendix A) to examine if the $1000-1330$ LT differences in tropospheric NO$_2$ columns observed by SCIAMACHY versus OMI are consistent with our understanding of diurnal variations in NO$_x$ emissions and chemical loss. Conceptually, and in the absence of transport, equation (3) shows that diurnal variation of tropospheric NO$_2$ columns (N_v) depends on the diurnal cycle of NO$_x$ emissions and chemical loss:

$$\frac{dN_v}{dt} = \alpha(t)(E(t) - k(t)N_x(t)), \qquad (3)$$

with $\alpha(t)$ the NO$_2$:NO$_x$ column ratio, $E(t)$ the NO$_x$ emission strength, and $k(t)$ the chemical loss rate constant for NO$_x$ columns $N_x(t)$ as a function of time of day t. Figure 6 conceptually illustrates the normalized diurnal variation of $N_v(t)$, $\alpha(t)$, $E(t)$ and $k(t)$ for a typical fossil fuel source region, where $k(t)$ mainly represents the chemical loss of NO$_x$ to HNO$_3$ (through the gas phase NO$_2$ + OH reaction
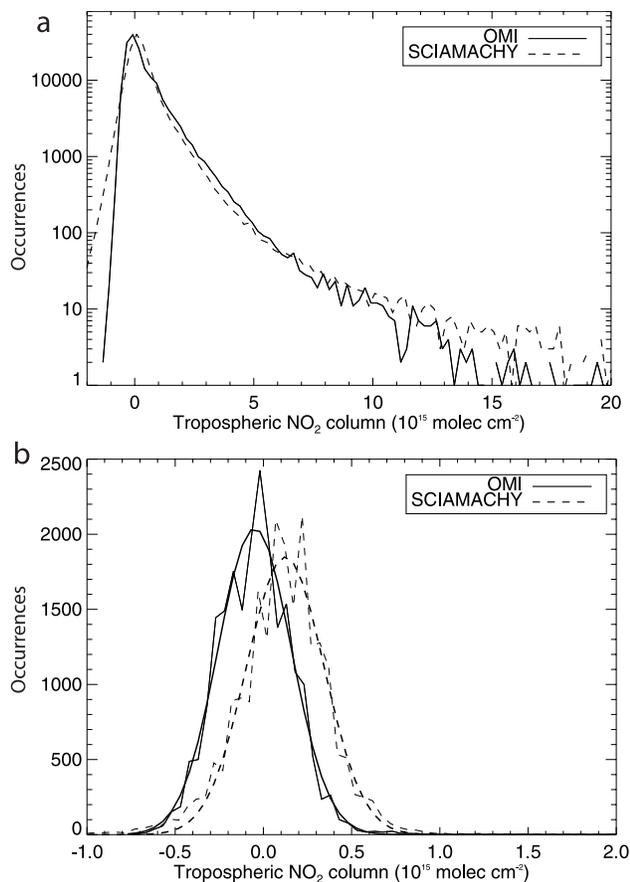
Figure 4. (a) Global probability distribution functions of monthly mean tropospheric NO$_2$ columns for SCIAMACHY and OMI in August 2006. (b) Subset for the Pacific Ocean (180–90°W, 45°S–15°N) only and Gaussian curves fitted to the data.

and by hydrolysis of N$_2$O$_5$ in aerosols). Since $\alpha(t)$ shows little difference between 1000 and 1330 LT, NO$_2$ columns increase in time if emissions add more NO$_x$ to the atmosphere than is chemically lost through $k(t)N_x(t)$. Chemical loss occurs throughout the diurnal cycle but is strongest at midday, when OH concentrations are highest. Over urban regions, emissions show a broad daytime maximum ($E(t)$ represents the U.S. mean diurnal variation from the *U.S. Environmental Protection Agency* [1989] in 4-h steps as applied worldwide in GEOS-Chem), whereas the integrated chemical loss between 1000 and 1330 LT is larger than the diurnal average, so that we expect NO$_2$ columns to be higher at 1000 LT than at 1330 LT. Over regions dominated by biomass burning or soil NO$_x$ emissions, $E(t)$ is likely higher in the afternoon than in the morning, and 1000–1330 LT column differences are expected to be smaller than over urban regions or even negative. The GEOS-Chem CTM includes all of the processes described above together with transport for a description of how NO$_2$ tropospheric columns would be expected to vary between 1000 and 1330 LT on the basis of current understanding.

5.2. Diurnal Variation in NO$_2$ Columns Over Fossil Fuel Source Regions

[33] We compare the GEOS-Chem simulated diurnal variations in tropospheric NO$_2$ columns to the OMI-SCIAMACHY results for the different NO$_x$ source regions in Figure 2. The diurnal cycle of emissions is shown in blue in Figure 7 (left): strongest emissions take place between 0600 and 1800 LT, related to highest anthropogenic activity, without much variation within that time frame.

[34] For observations and simulations to be comparable at the GEOS-Chem horizontal resolution of 2° latitude × 2.5° longitude, we require that 2° × 2.5° grid cells are sampled only on days when more than 50% of the (2° × 2.5°) geographical cell area was covered by SCIAMACHY and OMI observations with (observed) cloud radiance fractions <50%. This corresponds to more than 52 OMI pixels and more than 14 SCIAMACHY pixels within a 2° × 2.5° grid cell. The standard deviations of the (monthly, regional) mean tropospheric columns have been taken as the uncertainties of the SCIAMACHY and OMI observations.

[35] Figure 7 (left) shows the average diurnal cycle of tropospheric NO$_2$ columns simulated by GEOS-Chem and observed by SCIAMACHY and OMI over the northeastern United States for August 2006. NO$_2$ columns in the simulation with constant emissions show a minimum in the late afternoon, reflecting the diurnal cycle of chemical loss. The standard simulation with diurnally varying emissions has a weaker minimum a few hours earlier, and a less pronounced diurnal cycle (1000–1330 LT ratio 1.31, constant emissions: 1.59). It agrees better with the SCIAMACHY (1.18 ± 0.06) versus OMI (1.0 ± 0.05) observations. The observed ratio of 1.18 is significantly different from 1.0 given the uncertainties of the satellite instruments.

[36] Table 3 summarizes the results for all fossil fuel source regions at northern midlatitudes of Figure 2. GEOS-Chem simulates a 1000–1330 LT NO$_2$ column ratio of 1.3 for all regions, reflecting the model uniformity in the diurnal cycle of fossil fuel emissions and the similarity in the chemistry. It overestimates the observed 1000–1330 LT ratios in the northeastern United States and northern Europe, reproduces observations in northeastern China, and gets the trend wrong in the southeastern United States where the observed ratio is less than 1. The discrepancy between model and observations is larger over Europe than over the northeastern Unites States and China, possibly because of the relatively few days with cloud-free observations in August 2006 over Europe (SCIAMACHY 1.05 ± 0.09 and OMI 1.0 ± 0.08), compared to the northeastern United States and China.

[37] For comparison, we analyze the diurnal trend of observed surface NO$_2$ concentrations observed at EPA Aerometric Information Retrieval System (AIRS) urban sites for the summer of 2006. For six stations in the northeastern United States (Chicago, Detroit, Duluth, New York, Pittsburgh, and Philadelphia), the average 1000–1300 LT ratio in surface NO$_2$ concentrations is 1.43, close to the August 2006 GEOS-Chem ratio of tropospheric NO$_2$ columns. A 1000–1330 LT ratio >1.0 has also been found in summertime tropospheric NO$_2$ columns obtained with DOAS zenith-sky observations in Bologna, Italy [*Petritoli et al.*, 2005], especially during weekdays.
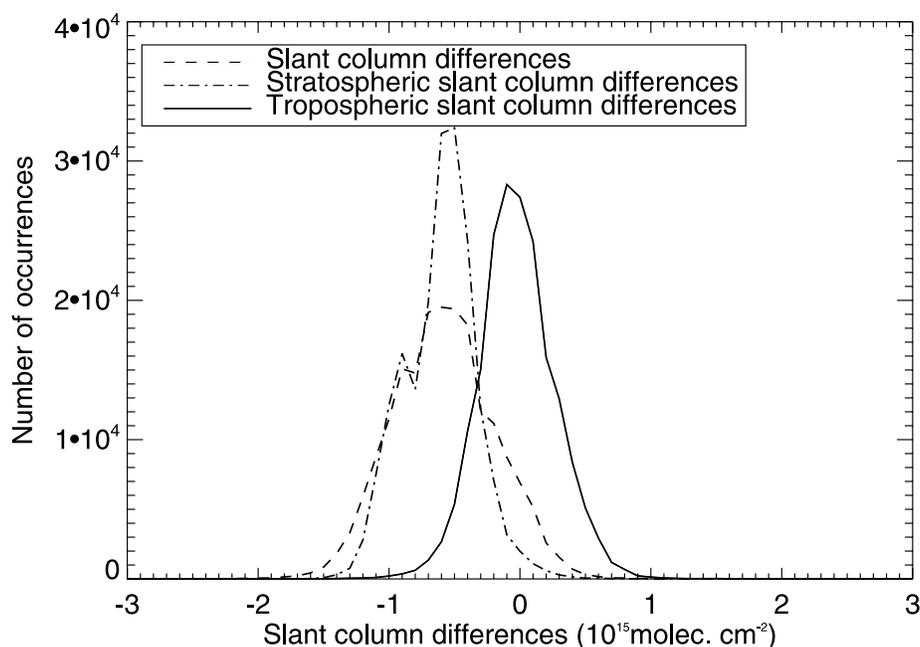
Figure 5. Distribution of SCIAMACHY-OMI differences in total slant columns (dashed line), in stratospheric slant columns (dashed-dotted line), and in tropospheric slant columns (solid line) for August 2006. All slant columns have been normalized by their geometrical air mass factors.

[38] The larger simulated than observed 1000–1330 LT ratio over the northern United States can likely be reconciled with an improved diurnal cycle of emissions that has recently become available. Figure 7 compares summertime normalized hourly emissions from the EPA National Emissions Inventory 2001 over the northeastern United States with the 4-h diurnal variation from the *U.S. Environmental Protection Agency* [1989] used in GEOS-Chem. In NEI2001, the emissions in the hours before 1000 LT are lower than in the hours before 1330 LT, whereas they are similar in the work by *U.S. Environmental Protection Agency* [1989], implying a smaller 1000–1330 LT ratio with the improved diurnal cycle of emissions (equation (3)).

[39] Urban areas in the southeastern United States (Houston, Dallas, and Atlanta, see Figure 2) show a GEOS-Chem

1000–1330 LT ratio >1.0, similar to the other fossil fuel regions. But for most of the rural Southeast, observed NO$_2$ is lower at 1000 LT than at 1330 LT. We hypothesize that the opposite diurnal variation between the observed (0.70) and modeled (1.31) 1000–1330 LT ratios over the southeastern United States likely reflects a different diurnal pattern of emissions in the rural Southeast in summer. The most important NO$_x$ sources in the rural Southeast are power plants, soils, biomass burning, and lightning. According to CEM (Continuous Emission Monitoring by the U.S. EPA) data for August 2006, the third warmest August since instrumental records began (NOAA, http://www.ncdc.noaa.gov/oa/climate/research/2006/aug/national.html), NO$_x$ power plant emissions in the southeastern United States are highest in the afternoon. Soil NO$_x$

Table 3. The 1000–1330 LT Ratios of Tropospheric NO$_2$ Columns for Selected Source Regions[a]

Region[b]	Corner Coordinates	Observed Column	Normalized Slant Column[c]	Normalized AMF[c]	Simulation: Standard Run[d]	Simulation: Constant Emissions[e]	Simulation: Diurnal Biomass Burning[f]
Northeastern U.S.	37–45°N, 71.25–86.25°W	1.18	1.06	0.90	1.31	1.59	1.31
Northern Europe	45–53°N, 1.25°W–23.75°E	1.05	1.03	0.98	1.30	1.50	1.30
Northeastern China	29–43°N, 103.75–123.75°E	1.37	1.25	0.91	1.29	1.46	1.29
Southeastern U.S.	29–35°N, 101.25–81.25°W	0.70	0.72	1.07	1.29	1.44	1.29
Southern Africa	17–7°S, 18.75–36.25°E	0.69	0.65	0.94	1.50	1.50	0.84
Brazil	17–3°S, 63.75–43.75°W	0.65	0.59	0.90	1.67	1.67	0.89
Indonesia	5°S–1°N, 101.25–116.25°E	0.63	0.62	1.01	1.76	1.76	1.02

[a]Monthly mean values for August 2006.

[b]Regions as indicated in Figure 2.

[c]Tropospheric NO$_2$ slant columns and tropospheric AMFs have been normalized by geometrical AMFs to correct for differences in viewing angles between SCIAMACHY and OMI as discussed in the text.

[d]Standard GEOS-Chem simulation with diurnally varying anthropogenic emissions and constant biomass burning emissions.

[e]GEOS-Chem simulation with all emissions constant in time.

[f]GEOS-Chem simulation with diurnally varying anthropogenic [*U.S. Environmental Protection Agency*, 1989] emissions and biomass burning emissions (Figure 7).
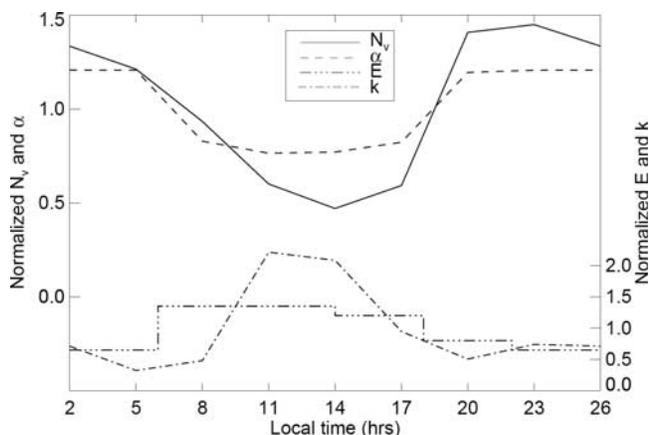
Figure 6. Conceptual illustration of the diurnal variation of the tropospheric NO$_2$ column (N_v), NO$_2$:NO$_x$ column ratio ($\alpha(t)$), NO$_x$ emissions ($E(t)$), and chemical loss rate constant (k) for NO$_x$ columns (see equation (3)) in a typical fossil fuel source region (August). Chemical loss of NO$_x$ takes mainly place by the gas phase NO$_2$ + OH reaction and by hydrolysis of N$_2$O$_5$ in aerosols. The left y axis holds for N_v and α, and the right y axis holds for $E(t)$ and $k(t)$.

emissions (dependent on soil temperature) are strongest in the afternoon [*Ludwig et al.*, 2001], and there is evidence that these emissions are significantly underestimated in the model [*Jaeglé et al.*, 2005]. Furthermore, *Park et al.* [2007] found strong biomass burning activity throughout the Southeast and GEOS-Chem does not take into account the diurnal cycle of fires (see next section). In summary, all

these NO$_x$ sources have a strong afternoon maximum and either their source strength (soils, lightning [*Hudman et al.*, 2007]) or their diurnal cycle (power plants, biomass burning) is underestimated. The observed 1000–1330 LT ratios <1.0 over the southeastern U.S. appear consistent throughout the summer as we also found them for July 2006 (not shown), while we did not find them for the nonsummer month of October 2004 (not shown). Obviously, there is a need for more aloft measurements to help explain the differences between simulated and observed 1000–1330 LT differences in NO$_2$ over the southeastern United States.

5.3. Diurnal Variation in NO$_2$ Columns Over Biomass Burning Regions

[40] High NO$_2$ columns in southern Africa, Brazil, and Indonesia in Figure 1 reflect considerable biomass burning activity during the local dry season. Biomass burning dominates over soil NO$_x$ emissions or lightning NO$_x$ production in the dry season [*Jaeglé et al.*, 2005]. In these regions, NO$_2$ columns from OMI are higher than from SCIAMACHY, but the standard GEOS-Chem simulation with no diurnal variation in biomass burning emissions shows the reverse. Recent satellite- and ground-based observations have shown that there is a distinct and consistent diurnal cycle in the agricultural practices driving tropical biomass burning [*Prins et al.*, 1998; *Kauffman et al.*, 2003; *Giglio et al.*, 2003] with a minimum at night and a maximum in the early to late afternoon. Therefore we implemented a diurnal cycle for biomass burning emissions in GEOS-Chem. This cycle is based on hourly fire counts over Central America detected by the Geostationary Operational Environmental Satellite (GOES-8) for 2002 [*Wang*
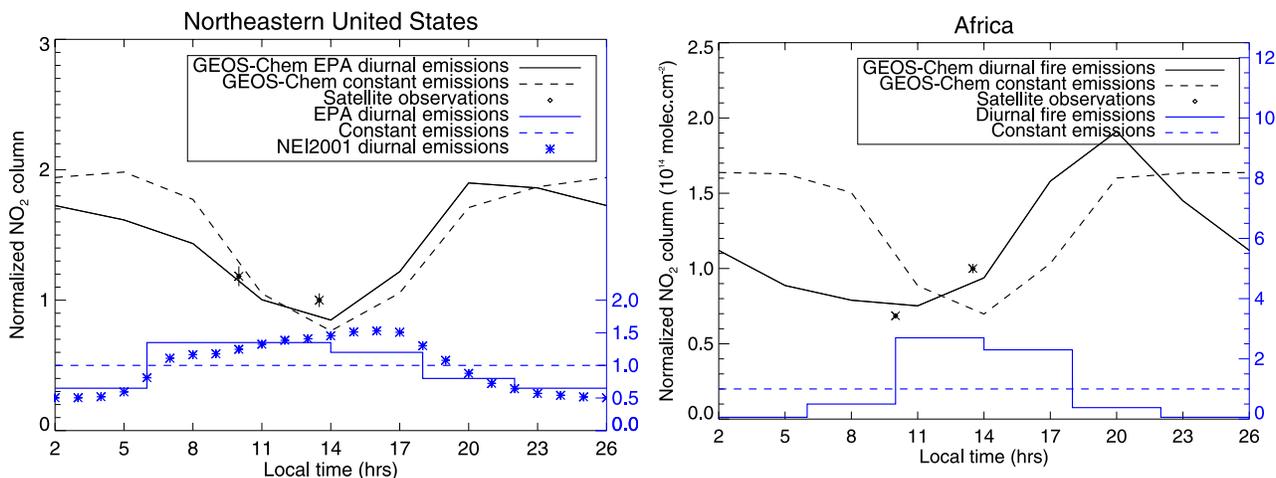

Figure 7. Average diurnal variation of tropospheric NO$_2$ columns modeled by GEOS-Chem (black lines) and observed by SCIAMACHY at 1000 LT and OMI at 1330 LT (diamond symbols) for the (left) northeastern U.S. and (right) African regions of Figure 2 in August 2006. Tropospheric NO$_2$ columns are normalized relative to the observed 1330 LT value. The error bars correspond to the standard deviation of the regional monthly mean tropospheric NO$_2$ columns. The solid line indicates the GEOS-Chem simulation with diurnal variations in NO$_x$ emissions. The dashed line indicates the GEOS-Chem simulation with constant emissions over the diurnal cycle. The solid blue lines show the diurnal variation of anthropogenic NO$_x$ emissions from the *U.S. Environmental Protection Agency* [1989] (left) and the diurnal variation of biomass burning emissions based on GOES fire counts [*Wang et al.*, 2006]. The blue dashed lines show constant emissions.

et al., 2006] and it is consistent with the diurnal distribution of fires observed by GOES-8 over South America in August 1995 [*Prins et al.*, 1998]. The 4-h normalized emission factors that we adopted are shown in blue in Figure 7 (right).

[41] Figure 7 (right) also shows the diurnal variation of NO₂ columns over southern Africa in August 2006, modeled by GEOS-Chem versus observed by SCIAMACHY (0.69 ± 0.02) and OMI (1.0 ± 0.03). We see that GEOS-Chem is able to reproduce the observed 1000–1330 LT increase by accounting for the diurnal variation of emissions. Table 3 shows that similar results are obtained over Brazil and Indonesia, though the simulated 1000–1330 LT ratio is still not as low as observed, possibly because even stronger diurnal variability needs to be included in biomass burning emissions [*Wang et al.*, 2006].

[42] A number of studies [*Martin et al.*, 2003; *Müller and Stavrakou*, 2005; *Jaeglé et al.*, 2005] have used GOME or SCIAMACHY NO₂ observations in the 1000–1030 LT window as top-down constraint on NO$_x$ emissions from biomass burning. These studies report emission estimates lower than bottom-up estimates based on carbon burned and NO$_x$ emission ratios, but this likely reflects the unaccounted diurnal variation of fire emissions. A midmorning overpass time is suboptimal for the observation of fires, and any top-down analysis needs to account for the large diurnal variation of fire emissions. Using our imposed diurnal cycle in Figure 7 (right), we find that a top-down constraint on biomass burning emissions based on 1000 LT observations would have to be corrected upward by 35% to account for this diurnal cycle. This difference is of the same order as the decreases reported on by *Martin et al.* [2003] and *Müller and Stavrakou* [2005], which supports the a priori inventories (6–7 Tg N a^{-1} globally) that they used, rather than the a posteriori optimized values that they derived.

6. Summary and Conclusions

[43] We have compared satellite retrievals of tropospheric NO₂ columns from two different instruments (SCIAMACHY and OMI) using similar retrieval methods for August 2006. The purpose of this comparison is to (1) gain confidence in the OMI near-real-time NO₂ data product (available from http://www.temis.nl), (2) examine if OMI NO₂ data can continue the long-term record of tropospheric NO₂ columns initiated by GOME and SCIAMACHY to monitor NO$_x$ emission trends, and (3) examine the information offered by satellite NO₂ observations at different times of day as additional constraint on the type and diurnal variation of NO$_x$ emissions. An essential difference between SCIAMACHY and OMI observations is that they are taken at different times of day (SCIAMACHY, 1000 LT; OMI, 1330 LT).

[44] The comparison of SCIAMACHY and OMI retrievals for locations and days when both instruments observed mostly clear scenes (less than 50% cloud radiance fraction) shows that the instruments observe similar spatial patterns of NO₂ (r = 0.77). Differences between SCIAMACHY and OMI outside of the major source areas (tropospheric NO₂ column <5.0 × 10¹⁵ molecules cm⁻²) are generally within the measurement uncertainties of both instruments (1.0–2.0 × 10¹⁵ molecules cm⁻²). We find evidence for a low

bias of approximately 0.2 × 10¹⁵ molecules cm⁻² in the OMI retrievals over oceans.

[45] SCIAMACHY observes higher NO₂ than OMI (up to 40%) in most industrial regions of northern midlatitudes, while it observes lower NO₂ than OMI (up to 35%) in tropical biomass burning regions. We show that these observed differences are not due to retrieval errors. Most of the difference is in the slant column, which simply reflects spectral fitting. There is also some contribution from the air mass factor (AMF) describing mixed layer growth from 1000 to 1330 LT, but it is small (typically less than 10%) and in any case it has some physical basis. Cloud-top pressures in OMI are 60 hPa lower than in SCIAMACHY, which can lead to some small AMF differences; these are difficult to characterize and are generally less than 10%.

[46] We used a global 3-D chemical transport model (GEOS-Chem) to interpret the 1000–1330 LT diurnal trends in NO₂ columns seen by SCIAMACHY and OMI as driven by diurnal variations in chemistry and emissions. Chemistry alone would cause higher NO₂ columns by a factor of 1.5 at 1000 LT compared to 1330 LT over source regions in the tropics and in midlatitudes summer, reflecting the photochemical sink from oxidation by OH. We find from GEOS-Chem that this diurnal variation is dampened by typically a third due to diurnal variation in fossil fuel emissions with a broad daytime maximum. This decrease is consistent with the 20–40% decrease observed between SCIAMACHY and OMI for the same days and locations, and furthermore with the 1000–1300 LT decrease in NO₂ surface concentrations observed by AIRS in summertime urban regions over the northeastern United States. Over urban regions in the southeastern United States, SCIAMACHY and OMI observe a 1000–1330 LT decrease that is similar to the other fossil fuel source regions. But over the Southeast, the observed 1000–1330 LT ratio (0.70) is opposite to the modeled (1.31). The most important NO$_x$ sources in the rural Southeast are power plants, soils, biomass burning, and lightning, and all these have strongest emissions in the afternoon. We hypothesize that these different diurnal patterns of emissions may explain the observed NO₂ column increase from 1000 to 1330 LT.

[47] The 35% increase in tropospheric NO₂ columns between 1000 and 1330 LT over tropical biomass burning regions is opposite to the diurnal cycle from photochemical loss. A diurnal cycle for biomass burning emissions that accounts for much stronger afternoon fire activity can resolve that discrepancy and is consistent with fire counts derived from geostationary satellite observations. Such a cycle is generally not included in chemical transport models but it should be. Top-down estimates on biomass burning NO$_x$ emissions based on NO₂ columns observed at 1000–1030 LT (SCIAMACHY, GOME) increase by 35% if the diurnal variation in fire emissions is taken into account. Previous studies that did not account for this diurnal variation in their top-down constraints incurred a corresponding error, leading them to the erroneous conclusion that prior bottom-up emission estimates were too high.

[48] Scaling factors between SCIAMACHY and OMI can be derived in order to continue trend analyses from GOME and SCIAMACHY into the OMI era. In future work, scaling factors (1000–1330 LT ratios) should be evaluated for the

complete seasonal cycle. There is a need to better understand the 1000–1330 LT ratios in terms of the diurnal variation in emissions (and possibly chemistry) in order to ensure continuity between the GOME, SCIAMACHY, and OMI tropospheric NO₂ data sets.

Appendix A: GEOS-Chem CTM

[49] For simulation of the diurnal variation of tropospheric NO₂ columns, we use the $2.5° \times 2.0°$ version of the 3-D chemical transport model GEOS-Chem (v7-04-06; http://www-as.harvard.edu/chemistry/trop/geos/index.html) [*Bey et al.*, 2001; *Park et al.*, 2004]. GEOS-Chem has been used previously for inverse modeling of NO_x emissions using GOME and SCIAMACHY satellite data by *Martin et al.* [2003], *Jaeglé et al.* [2005], *Martin et al.* [2006], and *Sauvage et al.* [2007] and we refer to these studies for more detailed descriptions of the model.

[50] GEOS-Chem is driven by assimilated meteorological fields (GEOS-4) from the NASA Global Modeling Assimilation Office (GMAO) that are provided every 6 h (3 h for surface fields and mixing depths). There are 55 vertical sigma levels, extending up from the surface to 0.01 hPa, and including 5 levels in the lowest 2 km of the atmosphere. The chemical simulations are conducted for August 2006 after a 7-month initialization.

[51] GEOS-Chem uses national emission inventories for anthropogenic NO_x where available, and otherwise default values from the Global Emission Inventory Activity (GEIA) [*Benkovitz et al.*, 1996] scaled to 1998 [*Bey et al.*, 2001]. For Europe we use the most recent NO_x emissions (2004) from the European Monitoring and Evaluation Program (EMEP) following *Auvray and Bey* [2005]. Over the U.S., (NO_x) emissions are taken from the EPA 1999 National Emissions Inventory (NEI99, *U.S. Environmental Protection Agency* [2001]). Over Mexico, emissions are from *Pitchford et al.* [2004]. The biomass burning inventory is based on satellite observations of fires by *van der Werf et al.* [2006], and emission factors from *Andreae and Merlet* [2001]. Soil NO_x emissions are computed following *Yienger and Levy* [1995] with canopy reduction factors described by *Wang et al.* [1998]. The production of NO_x by lightning is based on the cloud-top scheme of *Price and Rind* [1992] and vertical distribution from *Pickering et al.* [1998] with a global source of 4.7 Tg N a^{-1}.

[52] GEOS-Chem includes a detailed simulation of O_3-NO_x-hydrocarbon-aerosol chemistry. The aerosol and gaseous simulations are coupled through the formation of sulphate and nitrate, the HNO_3/NO_3^- partitioning of total inorganic nitrate, and the uptake of N_2O_5 by aerosols in the presence of water vapor (the main nighttime sink of NO_x, modeled as in the work by *Evans and Jacob* [2005]). The chemical time step in the model is 1 h, short enough to sample the 3.5 h time difference between the SCIAMACHY and OMI overpass times.

References

Acarreta, J. R., and P. Stammes (2005), Calibration comparison between SCIAMACHY and MERIS onboard ENVISAT, *IEEE Geosci. Remote Sens. Lett.*, 2(1), 31–35, doi:10.1109/LGRS.2004.838348.

Acarreta, J. R., J. F. De Haan, and P. Stammes (2004), Cloud pressure retrieval using the O₂-O₂ absorption band at 477 nm, *J. Geophys. Res.*, 109, D05204, doi:10.1029/2003JD003915.

Andreae, M. O., and P. Merlet (2001), Emission of trace gases and aerosols from biomass burning, *Global Biogeochem. Cycles*, 15, 955–966.

Auvray, M., and I. Bey (2005), Long-range transport to Europe: Seasonal variations and implications for the European ozone budget, *J. Geophys. Res.*, 110, D11303, doi:10.1029/2004JD005503.

Beirle, S., et al. (2006), Estimating the NO_x produced by lightning from GOME and NLDN data: A case study in the Gulf of Mexico, *Atmos. Chem. Phys.*, 6, 1075–1089.

Benkovitz, C. M., M. T. Scholtz, J. Pacyna, L. Tarrason, J. Dignon, E. C. Voldner, P. A. Spiro, J. A. Logan, and T. E. Graedel (1996), Global gridded inventories for anthropogenic emissions of sulphur and nitrogen, *J. Geophys. Res.*, 101, 29,239–29,253.

Bergman, J. W., and M. L. Salby (1996), Diurnal variations of cloud cover and their Relationship to climatological conditions, *J. Clim.*, 9, 2802–2820.

Bertram, T. H., A. Heckel, A. Richter, J. P. Burrows, and R. C. Cohen (2005), Satellite observations of daily variations in soil NO_x emissions, *Geophys. Res. Lett.*, 32, L24812, doi:10.1029/2005GL024640.

Bey, I., D. J. Jacob, R. M. Yantosca, J. A. Logan, B. D. Field, A. M. Fiore, Q. Li, H. Y. Liu, L. J. Mickley, and M. G. Schultz (2001), Global modeling of tropospheric chemistry with assimilated meteorology: Model description and evaluation, *J. Geophys. Res.*, 106(D19), 23,073–23,095.

Blond, N., K. F. Boersma, H. J. Eskes, R. J. van der A, M. Van Roozendael, I. De Smedt, G. Bergamatti, and R. Vautard (2007), Intercomparison of SCIAMACHY nitrogen dioxide observations, in situ measurements and air quality modeling results over Western Europe, *J. Geophys. Res.*, 112, D10311, doi:10.1029/2006JD007277.

Boersma, K. F., E. J. Bucsela, E. J. Brinksma, and J. F. Gleason (2002), NO₂, in *OMI Algorithm Theoretical Basis Document*, vol. 4, *OMI Trace Gas Algorithms*, ATB-OMI-04, Version 2.0, edited by K. Chance, pp. 13–36, NASA Distrib. Active Archive Cent., Greenbelt, Md., Aug.

Boersma, K. F., H. J. Eskes, and E. J. Brinksma (2004), Error analysis for tropospheric NO₂ retrieval from space, *J. Geophys. Res.*, 109, D04311, doi:10.1029/2003JD003962.

Boersma, K. F., H. J. Eskes, E. W. Meijer, and H. M. Kelder (2005), Estimates of lightning NO_x production from GOME satellite observations, *Atmos. Phys. Chem.*, 5, 2311–2331.

Boersma, K. F., et al. (2007), Near-real time retrieval of tropospheric NO₂ from OMI, *Atmos. Chem. Phys.*, 7, 2103–2118.

Boersma, K. F., et al. (2008), Validation of OMI tropospheric NO₂ observations during INTEX-B and application to constrain NO_x emissions over the eastern United States and Mexico, *Atmos. Environ.*, doi:10.1026/j.atmosenv.2008.02.004, in press.

Bogumil, K., et al. (2003), Measurements of molecular absorption spectra with the SCIAMACHY Pre-Flight Model: instrument characterization and reference data for atmospheric remote-sensing in the 230–2380 nm region, *J. Photochem. Photobiol. A Chem.*, 157, 167–184.

Bovensmann, H., J. P. Burrows, M. Buchwitz, J. Frerick, S. Nöel, V. V. Rozanov, K. V. Chance, and A. P. H. Goede (1999), SCIAMACHY: Mission objectives and measurement modes, *J. Atmos. Sci.*, 56(2), 127–150.

Dentener, F., W. Peters, M. Krol, M. van Weele, P. Bergamaschi, and J. Lelieveld (2003), Interannual variability and trend of CH₄ lifetime as a measure of OH changes in the 1979–2003 period, *J. Geophys. Res.*, 108(D15), 4442, doi:10.1029/2002JD002916.

Dirksen, R., M. R. Dobber, R. Voors, and P. Levelt (2006), Pre-launch characterization of the Ozone Monitoring Instrument transfer function in the spectral domain, *Appl. Opt.*, 45(17), 3972–3981.

Eskes, H. J., and K. F. Boersma (2003), Averaging kernels for DOAS total-column satellite retrievals, *Atmos. Chem. Phys.*, 3, 1285–1291.

Evans, M. J., and D. J. Jacob (2005), Impact of new laboratory studies of N₂O₅ hydrolysis on global model budgets of tropospheric nitrogen oxi-

des, ozone, and OH, *Geophys. Res. Lett.*, *32*, L09813, doi:10.1029/2005GL022469.

Giglio, L., J. D. Kendall, and R. Mack (2003), A multi-year active fire dataset for the tropics derived from TRMM VIRS, *Int. J. Remote Sens.*, *24*(22), 4505–4525.

Herman, J. R., and E. A. Celarier (1997), Earth surface reflectivity climatology at 340–380 nm from TOMS data, *J. Geophys. Res.*, *102*, 28,003–28,011.

Holtslag, A. A. M., and C.-H. Moeng (1991), Eddy diffusivity and countergradient transport in the convective atmospheric boundary layer, *J. Atmos. Sci.*, *48*, 1690–1698.

Hudman, R. C., et al. (2007), Surface and lightning sources of nitrogen oxides in the United States: Magnitudes, chemical evolution, and outflow, *J. Geophys. Res.*, *112*, D12S05, doi:10.1029/2006JD007912.

Jaeglé, L., R. V. Martin, K. V. Chance, L. Steinberger, T. P. Kurosu, D. J. Jacob, A. I. Modi, V. Yoboué, L. Sigha-Nkamdjou, and C. Galy-Lacaux (2004), Satellite mapping of rain-induced nitric oxide emissions from soils, *J. Geophys. Res.*, *109*, D21310, doi:10.1029/2004JD004787.

Jaeglé, L., L. Steinberger, R. V. Martin, and K. Chance (2005), Global partitioning of NOₓ sources using satellite observations: Relative roles of fossil fuel combustion, biomass burning and soil emissions, *Faraday Discuss.*, *130*, 407–423, doi:10.1039/b502128.

Kauffman, J. B., M. D. Steele, D. L. Cummings, and V. J. Jaramillo (2003), Biomass dynamics associated with deforestation, fire, and conversion to cattle pasture in a Mexican tropical dry forest, *For. Ecol. Manage.*, *176*, 1–12.

Kim, S.-W., A. Heckel, S. A. McKeen, G. J. Frost, E.-Y. Hsie, M. K. Trainer, A. Richter, J. P. Burrows, S. E. Peckham, and G. A. Grell (2006), Satellite-observed U.S. power plant NOₓ emission reductions and their impact on air quality, *Geophys. Res. Lett.*, *33*, L22812, doi:10.1029/2006GL027749.

Koelemeijer, R. B. A., P. Stammes, J. W. Hovenier, and J. F. de Haan (2001), A fast method for retrieval of cloud parameters using oxygen A-band measurements from the Global Ozone Monitoring Instrument, *J. Geophys. Res.*, *106*, 3475–3490.

Koelemeijer, R. B. A., P. Stammes, J. W. Hovenier, and J. F. de Haan (2002), Global distributions of effective cloud fraction and cloud top derived from oxygen A band spectra measured by the Global Ozone Monitoring Experiment: Comparison to ISCCP data, *J. Geophys. Res.*, *107*(D12), 4151, doi:10.1029/2001JD000840.

Konovalov, I. B., M. Beekmann, A. Richter, and J. P. Burrows (2006), Inverse modelling of the spatial distribution of NOₓ emissions on a continental scale using satellite data, *Atmos. Chem. Phys.*, *6*, 1747–1770.

Krol, M., S. Houweling, B. Bregman, M. van den Broek, A. Segers, P. van Velthoven, W. Peters, F. Dentener, and P. Bergamaschi (2005), The two-way nested global chemistry-transport zoom model TM5: Algorithm and applications, *Atmos. Chem. Phys.*, *5*, 417–432.

Levelt, P. F., G. H. J. van den Oord, M. R. Dobber, A. Mälkki, H. Visser, J. de Vries, P. Stammes, J. O. V. Lundell, and H. Saari (2006), The Ozone Monitoring Instrument, *IEEE Trans. Geosci. Remote Sens.*, *44*(5), 1093–1101.

Ludwig, J., F. X. Meixner, B. Vogel, and J. Förster (2001), Soil-air exchange of nitric oxide: An overview of processes, environmental factors, and modelling studies, *Biogeochemistry*, *52*, 225–257.

Martin, R. V., D. J. Jacob, K. Chance, T. P. Kurosu, P. I. Palmer, and M. J. Evans (2003), Global inventory of nitrogen oxide emissions constrained by space-based observations of NO₂ columns, *J. Geophys. Res.*, *108*(D17), 4537, doi:10.1029/2003JD003453.

Martin, R. V., C. E. Sioris, K. Chance, T. B. Ryerson, T. H. Bertram, P. J. Wooldridge, R. C. Cohen, J. A. Neuman, A. Swanson, and F. M. Flocke (2006), Evaluation of space-based constraints on global nitrogen oxide emissions with regional aircraft measurements over and downwind of eastern North America, *J. Geophys. Res.*, *111*, D15308, doi:10.1029/2005JD006680.

Martin, R. V., B. Sauvage, I. Folkins, C. E. Sioris, C. Boone, P. Bernath, and J. R. Ziemke (2007), Space-based constraints on the production of nitric oxide by lightning, *J. Geophys. Res.*, *112*, D09309, doi:10.1029/2006JD007831.

Müller, J.-F., and T. Stavrakou (2005), Inversion of CO and NOₓ emissions using the adjoint of the IMAGES model, *Atmos. Chem. Phys.*, *5*, 1157–1186.

Palmer, P. I., D. J. Jacob, K. Chance, R. V. Martin, R. J. D. Spurr, T. P. Kurosu, I. Bey, R. Yantosca, A. Fiore, and Q. Li (2001), Air-mass factor formulation for spectroscopic measurements from satellites: Application to formaldehyde retrievals from the Global Ozone Monitoring Experiment, *J. Geophys. Res.*, *106*, 14,539–14,550.

Park, R. J., D. J. Jacob, B. D. Field, R. M. Yantosca, and M. Chin (2004), Natural and transboundary pollution influences on sulphate-nitrate-ammonium aerosols in the United States: Implications for policy, *J. Geophys. Res.*, *109*, D15204, doi:10.1029/2003JD004473.

Park, R. J., D. J. Jacob, and J. A. Logan (2007), Fire and biofuel contributions to annual mean aerosol mass concentrations in the United States, *Atmos. Environ.*, *41*, 7389–7400.

Petritoli, A., E. Palazzi, C. Volta, and G. Giovanelli (2005), Validation of NO₂ tropospheric column from space in the Po valley (Italy), in *Tropospheric Sounding From Space ACCENT-TROPOSAT-2 in 2004–5*, edited by J. Burrows and P. Borrell, pp. 308–312, ACCENT Secr., Urbino, Italy.

Pickering, K. E., Y. Wang, W.-K. Tao, C. Price, and J.-F. Müller (1998), Vertical distributions of lightning NOₓ for use in regional and global chemical transport models, *J. Geophys. Res.*, *103*(D23), 31,203–31,216, doi:10.1029/98JD02651.

Pitchford, M. L., et al. (2004), Big Bend Regional Aerosol and Visibility Observational Study final report, U.S. Environ. Prot. Agency, Washington, D. C., Sept. (Available at http://vista.cira.colostate.edu/improve/Studies/BRAVO/reports/FinalReport/bravofinalreport.htm)

Price, C., and D. Rind (1992), A simple lightning parameterization for calculating global lightning distributions, *J. Geophys. Res.*, *97*, 9919–9933.

Prins, E. M., J. M. Feltz, W. P. Menzel, and D. E. Ward (1998), An overview of GOES-8 diurnal fire and smoke results for SCAR-B and 1995 fire season in South America, *J. Geophys. Res.*, *103*(D24), 31,821–31,835, doi:10.1029/98JD01720.

Richter, A., J. P. Burrows, H. Nüss, C. Granier, and U. Niemeier (2005), Significant increases in tropospheric nitrogen dioxide over China observed from space, *Nature*, *437*, 129–132, doi:10.1038/nature04092.

Sauvage, B., R. V. Martin, A. van Donkelaar, X. Liu, K. Chance, L. Jaeglé, P. I. Palmer, S. Wu, and T.-M. Fu (2007), Remote sensed and in situ constraints on processes affecting tropical tropospheric ozone, *Atmos. Chem. Phys.*, *7*, 815–838.

Schaub, D., D. Brunner, K. F. Boersma, J. Keller, D. Folini, B. Buchmann, H. Berresheim, and J. Staehelin (2007), SCIAMACHY tropospheric NO₂ over Switzerland: Estimates of NOₓ lifetimes and impact of the complex Alpine topography on the retrieval, *Atmos. Chem. Phys.*, *7*, 5971–5987.

Skupin, J., S. Noël, M. W. Wuttke, M. Gottwald, H. Bovensmann, M. Weber, and J. P. Burrows (2005), SCIAMACHY solar irradiance observation in the spectral range from 240 to 2380 nm, *Adv. Space Res.*, *35*(3), 370–375, doi:10.1016/j.asr.2005.03.036.

Stammes, P. (2001), Spectral radiance modeling in the UV-visible range, in *IRS2000: Current Problems in Atmospheric Radiation*, edited by W. L. Smith and Y. J. Timofeyev, pp. 385–388, A. Deepak, Hampton, Va.

Toenges-Schüller, N., O. Stein, F. Rohrer, A. Wahner, A. Richter, J. P. Burrows, S. Beirle, T. Wagner, U. Platt, and C. D. Elvidge (2006), Global distribution pattern of anthropogenic nitrogen oxide emissions: Correlation analysis of satellite measurements and model calculations, *J. Geophys. Res.*, *111*, D05312, doi:10.1029/2005JD006068.

U.S. Environmental Protection Agency (1989), The 1985 NAPAP emission inventory (version 2): Development of the annual data and modeler's tapes, *EPA-600/7-89-012a*, Research Triangle Park, N. C.

U.S. Environmental Protection Agency (2001), National air quality and emissions trends Report, 1999, *EPA 454/R-01-004*, Off. Of Air Qual. Plann. and Stand., Research Triangle Park, N. C.

Vandaele, A. C., C. Hermans, P. C. Simon, M. Carleer, R. Colin, S. Fally, M. F. Merienne, A. Jenouvrier, and B. Coquart (1998), Measurements of the NO₂ absorption cross-section from 42000 cm^{-1} to 10,000 cm^{-1} (238–1000 nm) at 220 K and 294 K, *J. Quant. Spectrosc. Radiat. Transfer*, *59*, 171–184.

van der A, R. J., D. H. M. U. Peters, H. Eskes, K. F. Boersma, M. Van Roozendael, I. De Smedt, and H. M. Kelder (2006a), Detection of the trend and seasonal variation in tropospheric NO₂ over China, *J. Geophys. Res.*, *111*, D12317, doi:10.1029/2005JD006594.

van der A, R. J., H. J. Eskes, M. Van Roozendael, I. De Smedt, N. Blond, K. F. Boersma, and A. Weiss (2006b), Algorithm document, Tropospheric NO₂ from satellites, *TEM/AD1/001*, R. Neth. Meteorol. Inst., De Bilt, Netherlands, Jan. (Available at http://www.temis.nl/airpollution/no2.html)

van der Werf, G. R., J. T. Randerson, L. Giglio, G. J. Collatz, P. S. Kasibhatla, and A. F. Arellano (2006), Interannual variability in global biomass burning emissions from 1997 and 2004, *Atmos. Chem. Phys.*, *6*, 3423–3441.

van Noije, T. P. C., et al. (2006), Multi-model ensemble simulations of tropospheric NO2 compared with GOME retrievals for the year 2000, *Atmos. Chem. Phys.*, *6*, 2943–2979.

Wang, J., S. A. Christopher, U. S. Nair, J. S. Reid, E. M. Prins, J. Szykman, and J. L. Hand (2006), Mesoscale modeling of Central American smoke transport to the United States: 1. "Top-down" assessment of emission strength and diurnal variation impact, *J. Geophys. Res.*, *111*, D14S92, doi:10.1029/2005JD006720.

Wang, Y., D. J. Jacob, and J. A. Logan (1998), Global simulation of tropospheric O₃-NOₓ-hydrocarbon chemistry: 1. Model formulation, *J. Geophys. Res.*, *103*, 10,713–10,726.

Yienger, J. J., and H. Levy (1995), Empirical model of global soil-biogenic NO$_x$ emissions, *J. Geophys. Res.*, *100*, 11,447–11,464.

————————————

K. F. Boersma, H. J. Eskes, and R. J. van der A, Royal Netherlands Meteorological Institute, NL-3730 AE De Bilt, Netherlands. (boersma@knmi.nl)

D. J. Jacob and J. Wang, School of Engineering and Applied Sciences, Harvard University, Pierce Hall, 29 Oxford Street, Cambridge, MA 02155, USA.

R. W. Pinder, Atmospheric Sciences Modeling Division, Air Resources Laboratory, NOAA/U.S. Environmental Protection Agency, Research Triangle Park, NC 27711, USA.